

Spatiotemporal reference evapotranspiration changes in humid and semi-arid regions of Iran: past trends and future projections

Milad Nouri¹ · Mehdi Homaei² · Mohammad Bannayan³

Received: 25 October 2016 / Accepted: 16 May 2017 / Published online: 17 June 2017
© Springer-Verlag Wien 2017

Abstract This study was undertaken to investigate the reference evapotranspiration (ET_0) changes in semi-arid and humid regions of Iran during the past (1966–2010) and future (2011–2099). For detecting possible trend in ET_0 over 1966–2010, the Mann–Kendall trend test was employed. The outputs of Hadley Centre coupled model version 3 (HadCM3) and the third generation couple global climate model (CGCM3) under A2, B2, and A1B emission scenarios were also used to simulate the future ET_0 changes by statistical downscaling model (SDSM). The results indicated upward trends in annual ET_0 during 1966–2010 in the most sites. Furthermore, the significant increasing ET_0 trends were identified for 54.5, 18.2, 27.3, 22.7, and 36.3% of studied locations during winter, spring, summer, autumn, and entire year, respectively. Positive trends in ET_0 were mostly found in north-east, west, and northwest Iran, and insignificant downward ET_0 trends were primarily detected in southwestern and southern stations in 1966–2010. The ET_0 changes were attributed to wind speed changes in semi-arid regions and mean temperature changes in humid areas in the past period. An increase in ET_0 was projected under all scenarios due mainly to temperature rise and declined relative humidity in the investigated regions from 2011 to 2100. Averaged over all stations, the lowest and highest ET_0 increment were, respectively, modeled

for autumn and summer using CGCM3 outputs and winter and autumn using HadCM3 outputs. Given significant ET_0 increase over the twenty-first century, appropriate adaptive measures are required to reduce negative impacts of climate change on water resources and agricultural productions.

1 Introduction

Since preindustrial period, increasing atmospheric concentrations of greenhouse gases (GHGs) and aerosols due primarily to fossil fuel overuse, land use/cover changes, and agricultural activities have triggered anthropogenic climate change (CC) and warming (IPCC 2013). Global climatic change impacts on atmospheric variables such as rainfall and temperature considerably affect the global mass and energy flux, e.g., the carbon cycle (Sarmiento et al. 1998) and the water cycle (Held and Soden 2006). Evapotranspiration which dominantly controls energy and mass transfers through interfaces of the soil–plant–atmosphere continuum (SPAC) plays key roles in the water and energy cycles (Seneviratne et al. 2010). Due to considerable complexities of measuring water flux through plants, crop evapotranspiration is mostly estimated based on reference crop evapotranspiration (Kite and Droogers 2000; Xie and Zhu 2013). Reference crop evapotranspiration, ET_0 , as defined by Allen et al. (1998) is the rate of evapotranspiration from a hypothetical reference crop which has an assumed height of 12 cm, a fixed surface resistance of 70 s m^{-1} , and an albedo of 0.23, mightily resembling evapotranspiration from an extensive surface of green grass with uniform height, actively growing, well-watered, and completely shading the ground. ET_0 expresses evaporative power of the atmosphere without being conditioned by soil physical condition and water availability. ET_0 is of great importance in estimating crop water requirement and scheduling, planning, and managing irrigation systems (Godfray et al. 2010; Homaei et al.

✉ Mehdi Homaei
mhomaee@modares.ac.ir

¹ Department of Soil Science, Tarbiat Modares University, P.O. Box 14115-336, Tehran, Iran

² Department of Irrigation and Drainage, Tarbiat Modares University, P.O. Box 14115-336, Tehran, Iran

³ Ferdowsi University of Mashhad, Faculty of Agriculture, P.O. Box 91775-1163, Mashhad, Iran

2002a; Homaei et al. 2002b; Irmak et al. 2006). Therefore, the changes of ET_0 considerably influence crop water requirement and consequently water resource management. Furthermore, increased ET_0 as a result of global warming can result in long-term meteorological droughts and finally enhance the aridity particularly in vulnerable ecosystems such as marginal semi-arid regions (Rahimi et al. 2013; Wang et al. 2015; Zarghami et al. 2011). Assessing the ET_0 changes can clearly reflect climatic changes in a given area (Wang et al. 2015; Wang et al. 2013).

In recent years, coupled Atmosphere–Ocean General Circulation Models (AOGCMs) have become an effective tool for investigating future impacts of CC on the hydrological cycle components. However, their coarse spatial resolution and inability to represent subgrid-scale features such as topography, clouds, and land use still remain serious challenges for studying potential impacts of CC (Fowler et al. 2007). Hitherto, two main downscaling methods, i.e., statistical and dynamical, have been emerged to relate coarse-scale GCM outputs to local-scale atmospheric variables (Wilby et al. 2002). Being low-cost, mostly freely available, and simple, the statistical methods have been applied extensively worldwide (Wilby et al. 2002). Among all statistical methods, statistical downscaling model (SDSM) has been broadly used for simulating and downscaling a wide range of climatic variables and extremes (Wilby and Dawson 2013; Wilby et al. 2014). Evaporation and evapotranspiration have been also downscaled and projected by SDSM (Wilby et al. 2014). Wang et al. (2013) projected the ET_0 changes by SDSM across the Tibetan plateau for the period 2011–2099. Their results showed considerable increments in projected annual and seasonal ET_0 under all scenarios over the plateau in the twenty-first century. Li et al. (2012) reported that ET_0 in the Loess plateau (northern China) will increase by about 4, 7, and 12% during the 2020s (2011–2040), the 2050s (2041–2070), and the 2080s (2071–2099), respectively. Xu et al. (2014) found an upward trend for annual ET_0 due mainly to changes in solar radiation, relative humidity, and minimum temperature in Zhejiang Province, East China, during the early twenty-first century (i.e., 2011–2040). They also pointed out that predicted seasonal and annual ET_0 changes varied significantly. Further, Liu et al. (2017) reported an increment in ET_0 during 2015–2099 as a result of reduction in relative humidity and increase of solar radiation in the Huang-Huai-Hai Plain, China, whereas a downward trend in annual ET_0 was detected for the last five decades. An increase in ET_0 and ET_c (actual crop evapotranspiration or crop water requirement) and irrigation demand was projected by Zamani et al. (2016) over 2025–2054 for Ramhormoz Plain, a small region located in southwest Iran. Wilby and Harris (2006) also found that the ET_0 increment would occur continuously during the twenty-first century in the Thames River basin, UK. Yang et al. (2012) reported around 40% increase and 30% decrease of extreme pan evaporation during summer and winter, respectively, by

using SDSM in the 2071–2100 under A2 scenario over the Dongjiang River basin, China. Chu et al. (2010) also projected negligible change in pan evaporation using SDSM over 2011–2040 in the Haihe River basin, China.

Iran is located in the Middle East, and its climate is predominantly semi-arid and arid (Bannayan et al. 2010). Long-term trend analyses of precipitation (Golian et al. 2015) and temperature (Tabari and Hosseinzadeh Talaei 2011) over Iran indicate that the climate is changing rapidly in the country. Natural resources in semi-arid and humid regions of Iran due to CC and growing population are under significant pressure. Despite a number of studies addressing the spatiotemporal trend of ET_0 over Iran during the past 50 years (Dinpashoh et al. 2011; Hosseinzadeh Talaei et al. 2014; Kousari and Ahani 2012; Nouri et al. 2017a), no investigation has been conducted to project the future ET_0 variations due to CC using statistical downscaling scheme. Therefore, the aims of this study are (i) to analyze spatiotemporal trend of annual and seasonal ET_0 in humid and semi-arid regions of Iran over the period of 1966–2010 and (ii) to project spatiotemporal changes in annual and seasonal ET_0 during three 30-year time periods, i.e., the 2020s (2011–2040), the 2050s (2041–2070), and the 2080s (2071–2099) using statistical downscaling.

2 Materials and methods

2.1 Study area

Iran, as the main part of the Iranian Plateau, is located in southwest Asia forming a connection among Asia, Europe, and Africa continents. The Alborz in north and the Zagros in west are the most important mountain ranges of the country and are responsible for nonuniform distribution of humidity and precipitation leading to different climatic conditions. Rain-producing air masses predominantly enter from west and northwest of country and cause above-average precipitation in western half of Iran owing to the Zagros mountain chain geographical location (Sadeghi et al. 2002). The Alborz mountain range in northern Iran also acts as a long barrier blocking rain-producing systems flowing from the Caspian Sea to north of the country. Consequently, semi-arid Mediterranean climate mostly dominates in west and northwest, and humid and subhumid climates prevail in northern Iran. Since this investigation focuses on Iran semi-arid and humid regions, the study area contains north, northeast, and western half of Iran. The location of studied sites is presented in Fig. 1.

2.2 Data

Daily meteorological data of 22 stations (Fig. 1) were obtained from Iran Meteorological Organization (IRIMO) for the period 1966–2010 to estimate ET_0 based on Penman–Monteith

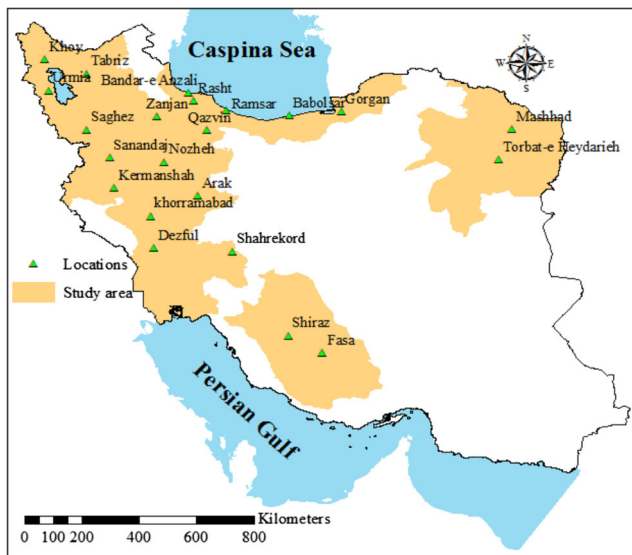


Fig. 1 The location of the investigated sites

FAO-56 (PMF-56) method. Geographic and climatic characteristics of all stations are given in Table 1. The dryness degree of climate at the surveyed stations was determined using UNEP (1997) aridity index:

$$AI = \frac{P}{ET_0} \tag{1}$$

where AI , P , and ET_0 are annual aridity index, precipitation (mm), and reference evapotranspiration (mm) (estimated based on the PMF-56 equation), respectively.

Regions with AI larger than 0.2 and 1.0 are classified as semi-arid and humid areas, respectively.

The observed coarse-resolution atmospheric variables (including 26 sets of data for each GCM), as the predictors, were derived from the National Centers for Environmental Prediction and National Center for Atmospheric Research (NCEP/NCAR) reanalysis dataset to calibrate and validate SDSM (Kistler et al. 2001). In addition, the outputs of the third version of Hadley Center coupled model (HadCM3) and the third generation of the coupled Canadian global climate model (CGCM3) were used to project future changes in ET_0 . Figure 2 depicts CGCM3 and HadCM3 grid points obtained from the Canadian Climate Change Scenarios Network (CCCSN) (<http://www.ccsn.ec.gc.ca>) over Iran. The IPCC emission scenarios applied in this study were A2, B2, and A1B. In this study, the scenarios considered for CGCM3 were A2 (CG3A2) and A1B (CG3A1B) and for HadCM3 model were A2 (HadA2) and B2 (HadB2).

2.3 The Penman–Monteith FAO-56 model

The most recommended form of PMF-56 was used in this study to determine reference crop evapotranspiration:

$$ET_0 = \frac{0.408\Delta(R_n - G) + \gamma \frac{900}{T_{mean} + 273} U(e_s - e_a)}{\Delta + \gamma(1 + 0.34U)} \tag{2}$$

where ET_0 is the reference crop evapotranspiration (mm day^{-1}), Δ is the slope of saturation vapor pressure curve ($\text{kPa } ^\circ\text{C}^{-1}$), R_n is the net radiation at the reference crop surface ($\text{MJ m}^{-2} \text{day}^{-1}$), G is the soil heat flux density ($\text{MJ m}^{-2} \text{day}^{-1}$), T_{mean} is the mean daily air temperature at 2-m height ($^\circ\text{C}$), U is the daily average wind speed at 2-m height (m s^{-1}), e_s is the saturation vapor pressure (kPa), e_a is the actual vapor pressure (kPa), $e_s - e_a$ is the saturation vapor pressure deficit (kPa), and γ represents the psychrometric constant ($\text{kPa } ^\circ\text{C}^{-1}$).

Since at some stations, sunshine duration data have been lacking or of poor quality (mainly for 1979–1982), the missing data were handled using the Hargreaves’ radiation model (Allen et al. 1998):

$$SR = K_{rs}R_a(T_{max} - T_{min})^{0.5} \tag{3}$$

where SR and R_a are the solar radiation and extraterrestrial radiation ($\text{MJ m}^{-2} \text{day}^{-1}$), T_{max} and T_{min} are the maximum and minimum daily air temperature ($^\circ\text{C}$), and K_{rs} represents an empirical coefficient which in interior and coastal regions is approximately equal to 0.16 and 0.19, respectively ($^\circ\text{C}^{-0.5}$).

2.4 Trend analysis

Nonparametric rank-based Mann–Kendall trend test was applied to temporally detect significant ET_0 variations. The Mann–Kendall test statistics is calculated by Yue et al. (2002):

$$S = \sum_{k=1}^{n-1} \sum_{j=k+1}^n \text{sign}(x_j - x_k) \tag{4}$$

$$\text{sign}(x_j - x_k) = \begin{cases} 1 & (x_j - x_k) > 0 \\ 0 & (x_j - x_k) = 0 \\ -1 & (x_j - x_k) < 0 \end{cases} \tag{5}$$

$$\text{Var}(S) = \left\{ [n(n-1)(2n+5)] - \left[\sum_{i=1}^m t_i(t_i-1)(2t_i+5) \right] \right\} / 18 \tag{6}$$

where S represents the Mann–Kendall statistics, n denotes data set length, x_j and x_k are the sequential data values, t_i is the number of ties of extent i , and m is the number of the tied groups.

The standardized Mann–Kendall test statistics (Z) which follows standard Gaussian distribution is then determined by

$$Z = \begin{cases} [S-1] / \sqrt{\text{Var}(S)} & S > 0 \\ 0 & S = 0 \\ [S+1] / \sqrt{\text{Var}(S)} & S < 0 \end{cases} \tag{7}$$

Table 1 Geographic characteristics, aridity index, and climate classification of the surveyed stations over the 1966–2010

WMO number	Station	Longitude (°E)	Latitude (°N)	Elevation (m a.s.l)	AI (-)	Climate (UNEP 1997)
40703	Khoy	44° 58'	38° 33'	1103.0	0.29	Semi-arid
40706	Tabriz	46° 17'	38° 05'	1361.0	0.20	Semi-arid
40712	Urmia	45° 05'	37° 32'	1315.9	0.29	Semi-arid
40718	Anzali	49° 28'	37° 28'	-26.2	2.06	Humid
40719	Rasht	49° 39'	37° 12'	36.7	1.62	Humid
40727	Saghez	46° 16'	36° 15'	1522.8	0.42	Semi-arid
40729	Zanjan	48° 29'	36° 41'	1663.0	0.26	Semi-arid
40731	Qazvin	50° 03'	36° 15'	1279.2	0.25	Semi-arid
40732	Ramsar	50° 40'	36° 54'	-20.0	1.51	Humid
40736	Babolsar	52° 39'	36° 43'	-21.0	1.02	Humid
40738	Gorgan	54° 16'	36° 51'	13.3	0.60	Dry subhumid
40745	Mashhad	59° 38'	36° 16'	999.2	0.20	Semi-arid
40747	Sanandaj	47° 00'	35° 20'	1373.4	0.36	Semi-arid
40762	Torbat-e heydariieh	59° 13'	35° 16'	1450.8	0.20	Semi-arid
40766	Kermanshah	47° 09'	34° 21'	1318.6	0.32	Semi-arid
40767	Nozheh	48° 43'	35° 12'	1679.7	0.23	Semi-arid
40769	Arak	49° 46'	34° 06'	1708.0	0.26	Semi-arid
40782	Khorramabad	48° 17'	33° 26'	1147.8	0.33	Semi-arid
40795	Dezful	48° 23'	32° 24'	143.0	0.25	Semi-arid
40798	Shahrekord	50° 51'	32° 17'	2048.9	0.28	Semi-arid
40848	Shiraz	52° 36'	29° 32'	1481.0	0.20	Semi-arid
40859	Fasa	53° 41'	28° 58'	1288.3	0.20	Semi-arid

WMO World Meteorological Organization

To calculate the relative changes of ET_0 during 1966–2010, the following equation was used:

$$RC = 100 \frac{nQ}{|\bar{x}|} \quad (8)$$

$$Q = \text{Median} \left[(x_i - x_j) / (t_i - t_j) \right] \text{ for } i = 1, \dots, n \quad (9)$$

where RC is relative change (%), n denotes the data set record length, Q represents the Sen's slope estimator (Sen 1968), \bar{x} is the average value of time series, and x_i and x_j are values of data in time series at times of t_i and t_j ($i > j$), respectively.

The Mann–Kendall trend test assumes that the observed time series are serially independent. However, the studies that assessed the trend in hydrometeorological variables have concluded that these series are mostly auto-correlated. As a result, some procedures have been proposed to produce serially independent time series required before using the Mann–Kendall test (Yue et al. 2002). In this study, prewhitening method introduced by von Storch (1999) was applied to remove serial correlation from the ET_0 series.

2.5 Contribution of climatic variables to the ET_0 dynamics

We used the detrending method to determine the contribution of mean temperature (T_{mean}), wind speed (U), relative humidity (RH), and solar radiation (SR) to the ET_0 variations. In order to implement the detrending procedure in the first step, the trend in the RH, SR, U and T_{mean} was removed and the time series became stationary (Xu et al. 2006). In order to

assess the contribution of a specific variable (for instance, U), ET_0 was then recalculated with the detrended data series (e.g., the detrended U series), while the original data set was used for other variables. Finally, the average difference between ET_0 calculated with original data and ET_0 recalculated with detrended data was computed. This difference quantifies the contribution of a specific variable to the ET_0 changes. The larger absolute difference indicates the higher contribution of a given variable to the ET_0 trend (Huo et al. 2013; Xu et al. 2006).

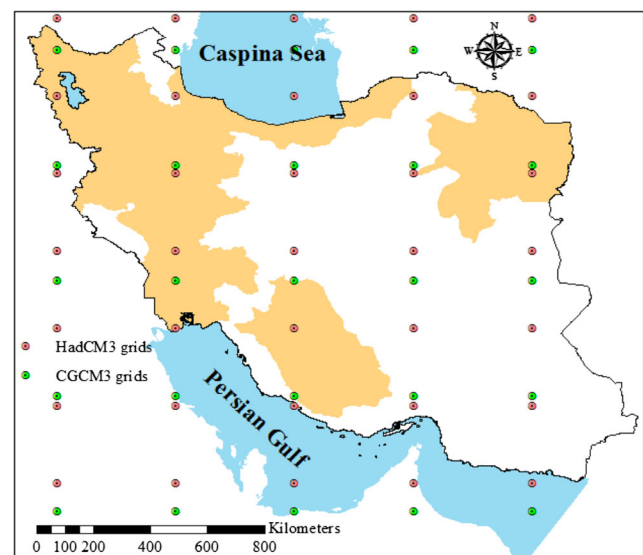


Fig. 2 The distribution of the GCM grid points over Iran

2.6 Statistical downscaling method

SDSM which is a combination of the regression-based and stochastic weather generator downscaling techniques (Wilby et al. 2002) was employed to establish statistical functions between the coarse-scale GCM output and local-scale atmospheric variables. There are two approaches to downscale multivariable factors such as ET_0 by SDSM (Wang et al. 2015). The ET_0 can be treated as an exotic variable and directly downscaled by SDSM. Alternatively, ET_0 can be estimated using the SDSM-downscaled controlling climatic factors (i.e., T_{mean} , U , RH , and SR) as inputs for ET_0 models (e.g., PMF-56). In this study, we used the first method. In order to statistically downscale coarse-scale data, the most correlated large-scale predictors (Table 2) were selected using “screen variables” operation of SDSM. This operation of the software provides some useful tools, i.e., explained variance, correlation matrix, partial correlation, and scatter plot for identifying appropriate large-scale independent variables of statistical functions. To calibrate monthly multiple linear regression functions (MLRs), 25-year (1966–1990) of daily NCEP/NCAR reanalysis data and calculated ET_0 series were used. The rest of the data (i.e., 1991–2001) was afterwards applied to validate the established MLRs. The developed models (MLRs) were then used to downscale the large-scale GCM outputs.

2.7 Quantitative evaluation of model performance

The SDSM performance in simulating ET_0 time series for the calibration and validation periods was assessed using three different statistics including normalized root mean square (nRMSE), mean bias error (MBE), and the Nash–Sutcliffe model efficiency coefficient (NSE). The mathematical expressions of these statistics are

$$MBE = \left[\frac{\sum_{i=1}^n (S_i - O_i)}{n} \right] \quad (10)$$

$$nRMSE = \frac{100}{O} \left[\sqrt{\frac{\sum_{i=1}^n (S_i - O_i)^2}{n}} \right] \quad (11)$$

$$NSE = \left[\frac{\sum_{i=1}^n (O_i - \bar{O})^2 - \sum_{i=1}^n (S_i - O_i)^2}{\sum_{i=1}^n (O_i - \bar{O})^2} \right] \quad (12)$$

where S_i is the simulated values, O_i is the observed values, \bar{O} is mean of the observations, and n is the number of time steps.

The nRMSE, as a measure of absolute error, is frequently used to characterize the differences between the simulated and recorded values in the agrohydrology literature (Dashtaki et al. 2010; Nouri et al. 2016). The model performance is considered perfect with the nRMSE value less than 10%, good if the nRMSE is between 10 and 20%, fair if the nRMSE is between

20 and 30%, and poor if the nRMSE quantity is greater than 30% (Dettori et al. 2011). The MBE, as a measure of systematic error, is an index quantifying model bias, and its negative (positive) values indicate model tendency to underestimate (overestimate) (Palosuo et al. 2011). The NSE (a goodness-of-fit statistics) quantifies the relative error and varies between 1.0 to minus infinity (Nash and Sutcliffe 1970). If the simulated values are equivalent to the observations ($S_i = O_i$), the model performance is excellent and the magnitude of NSE statistics is 1.0 and the quantity of the MBE and nRMSE is zero.

3 Results and discussions

3.1 The ET_0 trend analysis over 1966–2010

The relative change (%) and the Mann–Kendall trend test results for annual and seasonal ET_0 in the period of 1966–2010 are demonstrated in Fig. 3. In about 77.0% of the surveyed stations, the positive relative changes (trends) were found in annual ET_0 during 1966–2010. The significant trend in annual ET_0 time series was, however, identified in 36.3% of the stations based on the Mann–Kendall trend test at the 95% confidence level. The highest positive and negative change of annual ET_0 was also obtained at Gorgan (27.77%) and Dezful (−22.92%), respectively. Spatially, the trend of annual ET_0 in southern and southwestern locations (e.g., Fassa and Dezful) was insignificantly declining during 1966–2010. However, in north, northwest, northeast, and west of the country, there was an upward trend in annual ET_0 . On the seasonal scale, the ET_0 trends were increasing during winter, spring, summer, and autumn for 19, 16, 17, and 17 stations, respectively. In addition, about 54.5, 18.2, 27.3, and 22.7% of locations showed positive significant trend ($p \leq 0.05$) in winter, spring, summer, and autumn ET_0 , respectively. Therefore, more sites exhibited significant trend in winter ET_0 . Moreover, the ET_0 increments were mostly significant during wintertime in west and northwest Iran. Similar to annual scale, insignificant downward trends in seasonal ET_0 were detected for southwestern and southern sites. In some cases such as Qazvin and Zanjan as well as Dezful and Shahrekord stations, two adjacent locations showed inverse trends in ET_0 series. This can be explained by different microclimates caused by local wind circulation and physical topography at two nearby areas (Türkeş and Sümer 2004). The climate of west and northwest Iran is considerably impacted by mountain-plain winds and slope winds besides prevailing atmospheric circulations (Tabari and Hosseinzadeh Talaei 2011). In case of Shahrekord and Dezful, the Zagros Mountains lying between the sites and considerable elevation difference (almost 1900 m) leading to different microclimatic conditions can account for observed inverse trends in ET_0 of these two adjacent regions. These results are in agreement

Table 2 Candidate large-scale NCEP/NCAR predictors and the number of sites in which the predictors were selected

No.	Predictor	Selection	No.	Predictor	Selection
1	Mean sea-level pressure	16	15	850 hPa airflow strength	9
2	Surface airflow strength	2	16	850 hPa zonal velocity	10
3	Surface zonal velocity	6	17	850 hPa meridional velocity	2
4	Surface meridional velocity	3	18	850 hPa vorticity	3
5	Surface vorticity	1	19	850 hPa geopotential height	4
6	Surface wind direction	1	20	850 hPa wind direction	0
7	Surface divergence	2	21	850 hPa divergence	3
8	500 hPa airflow strength	6	22	Relative humidity at 500 hPa	2
9	500 hPa zonal velocity	11	23	Relative humidity at 850 hPa	8
10	500 hPa meridional velocity	8	24	Near-surface relative humidity	17
11	500 hPa vorticity	2	25	Surface specific humidity	6
12	500 hPa geopotential height	8	26	Mean temperature at 2 m	20
13	500 hPa wind direction	0	27	Specific humidity at 500 hPa	1
14	500 hPa divergence	2	28	Specific humidity at 850 hPa	5

with those reported by Dinpashoh et al. (2011), Kousari and Ahani (2012), and Hosseinzadeh Talaei et al. (2014).

3.2 Contribution analysis of ET₀ in 1966–2010

The average difference values (over 1966–2010) between annual and seasonal ET₀ calculated with original meteorological data (ET_{0-org}) and recalculated with detrended *U* (ET_{0-det,U}), *T*_{mean} (ET_{0-det,Tmean}), RH (ET_{0-det,RH}), SR (ET_{0-det,SR}), and all climatic data series (ET_{0-det,all}) are given in Fig. 4. The positive (negative) values suggest the positive (negative) effects of the trend in meteorological variables on the ET₀ trend. There were 17.8, −96.8, −4.2, and −30.0 mm year^{−1} differences (averaged over 1966–2010) between annual ET_{0-org} and ET_{0-det,Tmean}, ET_{0-det,U}, ET_{0-det,SR}, and ET_{0-det,RH}, respectively, in semi-arid regions with declining trend in annual ET₀ (Fig. 4). In other words, negative trend of annual ET₀ in Qazvin, Nozheh, Dezful, Shiraz, and Fassa (the sites experienced decreasing trend in ET₀ (Fig. 3)) is

majorly caused by declined *U*. Moreover, the average differences between annual ET_{0-org} and ET_{0-det,Tmean}, ET_{0-det,U}, ET_{0-det,SR}, and ET_{0-det,RH} were approximately 13.9, 54.9, −2.3, and 2.1 mm year^{−1}, respectively, for semi-arid regions with positive annual ET₀ trend. Therefore, the positive trend in annual ET₀ is mainly due to increase of *U* in the semi-arid sites with increasing trend in annual ET₀ (Fig. 3). As a result, one attributes the changes of annual ET₀ greatly to the *U* variations in semi-arid regions. Around 46.9 and 48.5% of difference between ET_{0-org} and ET_{0-det,all} is accounted for by summertime ET₀ differences in semi-arid regions with decreasing and increasing ET₀ trend, respectively. Consequently, it seems that summer ET₀ changes made a more important contribution to changes in annual ET₀ owing to greater changes of summer wind speed over the semi-arid regions. The highest average difference was calculated between ET_{0-org} and ET_{0-det,Tmean} (17.8 mm year^{−1}) followed by ET_{0-org} and ET_{0-det,RH} (13.6 mm year^{−1}) in humid regions. Hence, increasing trend in ET₀ is mostly attributable to enhanced *T*_{mean}

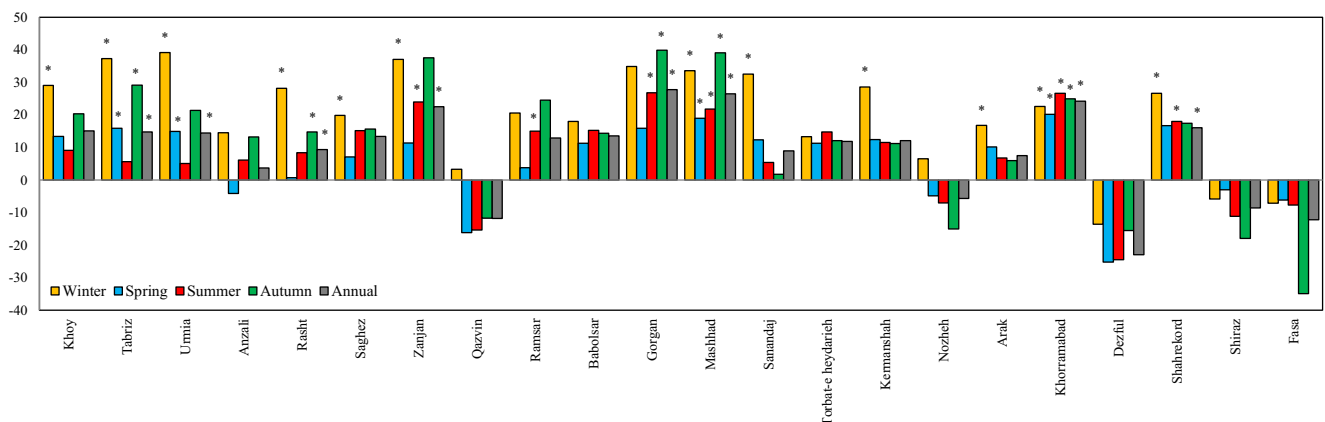


Fig. 3 Annual and seasonal ET₀ relative changes (%) for the studied stations over 1966–2010 Asterisks represent significant trends at the 95% confidence level

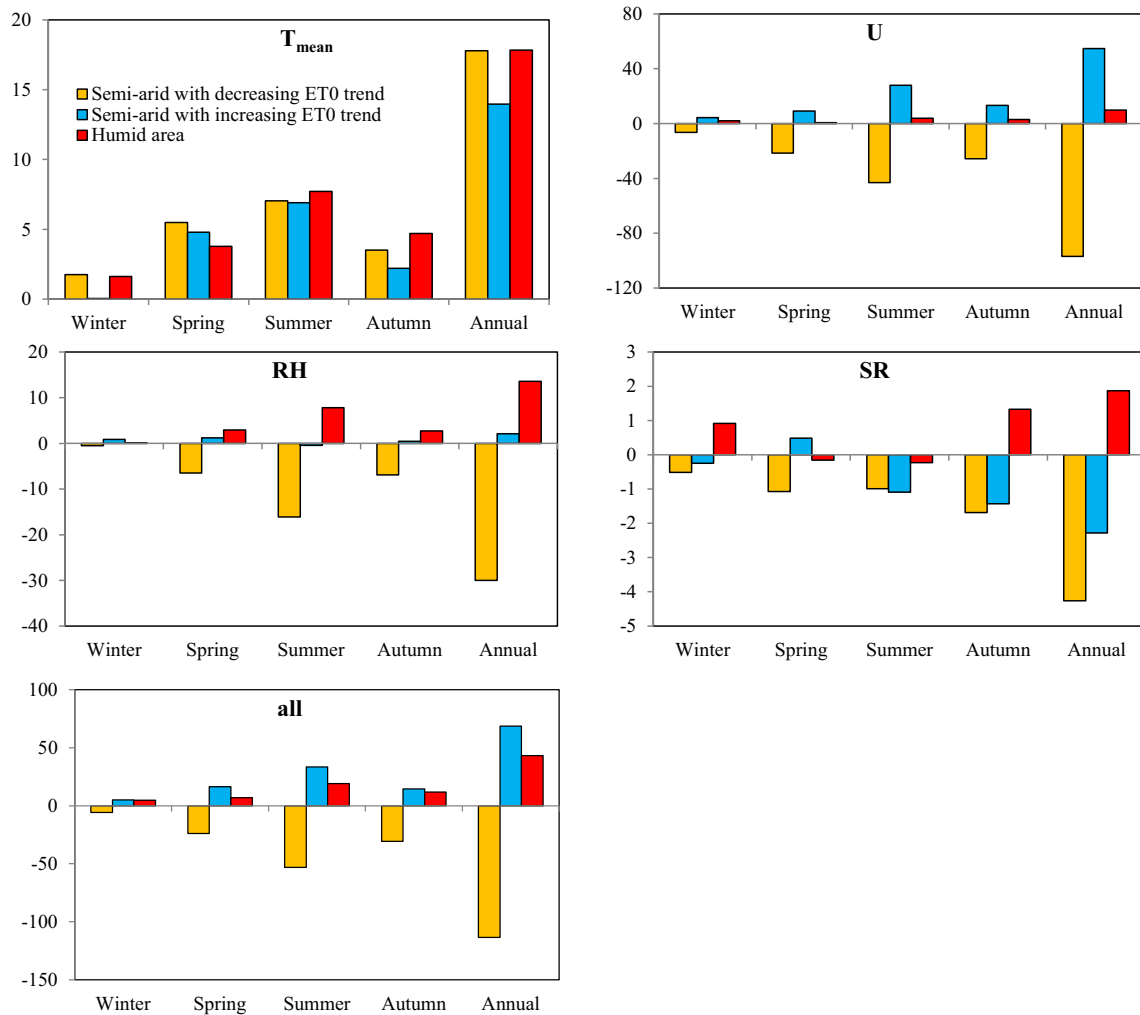


Fig. 4 The average differences between ET₀ calculated with original data and ET₀ recalculated with detrended T_{mean} , U , RH, SR, and all variable data (mm year⁻¹) for semi-arid regions with decreasing and increasing trends and humid areas

and also decreased RH in Rasht, Anzali, Ramsar, and Babolsar (the humid sites with positive annual ET₀ trend (Fig. 3)). Similar to semi-arid regions, summertime changes in climatic variables play more important role in the ET₀ variation of humid stations. Dinpashoh et al. (2011) concluded that T_{max} (maximum temperature) in Anzali (a humid area) and U in Mashhad, Nozheh, Tabriz, Sannandaj, and Shiraz (semi-arid regions) are the main contributors to the ET₀ changes using the stepwise regression analysis over 1965–2005. Our results are thus consistent with those reported by Dinpashoh et al. (2011). Nouri et al. (2017a) attributed the ET₀ changes to the U variations for most arid sites located in central, eastern, and southeastern Iran over the last five decades.

3.3 SDSM performance

As given in Table 2, mean temperature at 2 m (in about 91% of the stations), near-surface relative humidity (in around 77% of the sites), and mean sea-level pressure (in approximately 73%

of the locations) are the most relevant predictors used by SDSM to establish the MLRs. Some atmospheric circulation factors such as 850 hPa airflow strength, 500 hPa zonal velocity, 850 hPa zonal velocity, and 500 hPa meridional velocity were also employed at more than 35% of investigated sites (Table 2). Li et al. (2012) found that ET₀ (predictand) was more sensitive to mean temperature at 2 m, near-surface relative humidity, and relative humidity at 500 hPa (independent predictors) over the Loess Plateau of China. Wang et al.

Table 3 The statistic values, averaged across all locations, to evaluate SDSM performance

Period	GCM	nRMSE (%)	MBE (mm day ⁻¹)	NSE (-)
Calibration	HadCM3	0.43	0.14	1.00
	CGCM3	0.41	-0.01	1.00
Validation	HadCM3	5.87	0.38	0.98
	CGCM3	5.85	-0.50	0.99

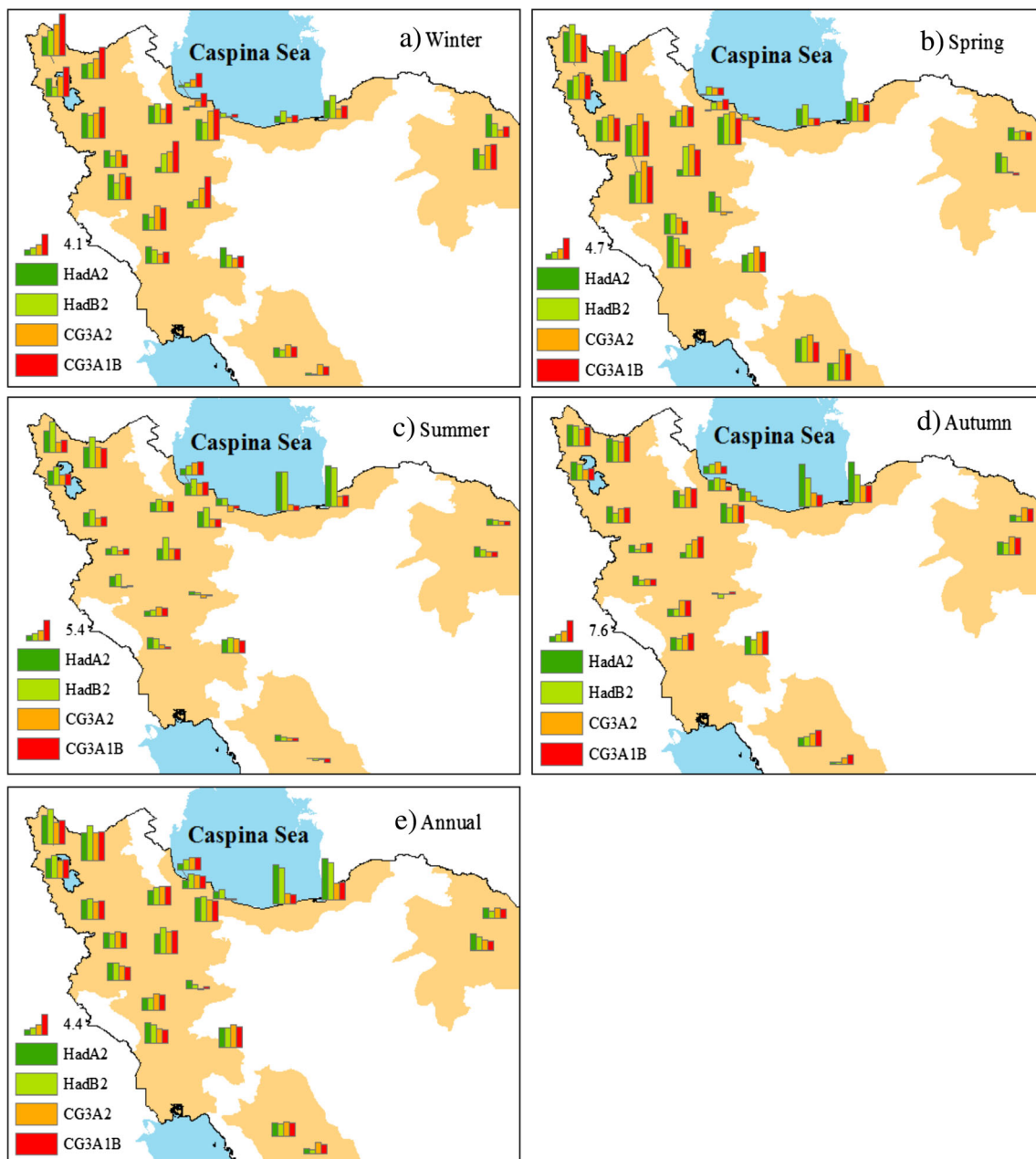


Fig. 5 The ET_0 changes (%) with respect to the baseline period in the study area under HadA2, HadB2, CG3A2, and CG3A1B scenarios in the 2020s

(2013) have also identified the highest association between ET_0 and mean temperature at 2 m, mean sea-level pressure, and 500 hPa geopotential height across the Tibetan Plateau, China. Therefore, it can be concluded that temperature-related and humidity-related large-scale predictors are of greater importance in simulating ET_0 by SDSM.

Given below 10% values of the nRMSE calculated for both GCMs (Table 3), SDSM performed perfect in estimating ET_0 (as an exotic variable) during both calibration (1966–1990) and validation (1991–2001) periods. The negative MBE magnitude reveals that SDSM slightly tended to underestimate when the CGCM3 outputs were used to generate the ET_0 series. On contrary, the model negligibly overestimated the

ET_0 when the HadCM3 outputs were employed. Over 0.98 values of the NSE (Table 3) indicate small relative error in synthesizing the ET_0 series by the established MLR functions. SDSM performed well in developing statistical downscaling functions (i.e., MLRs) by using both HadCM3 and CGCM3 data sets during the calibration and validation periods. SDSM thus appears to be capable of adequately simulating ET_0 series for the future in the study area.

3.4 Projection of future ET_0 changes

Averaged across all sites, there will be 2.65, 2.54, 3.18, and 3.14% increments in annual ET_0 for HadA2, HadB2, CG3A2,

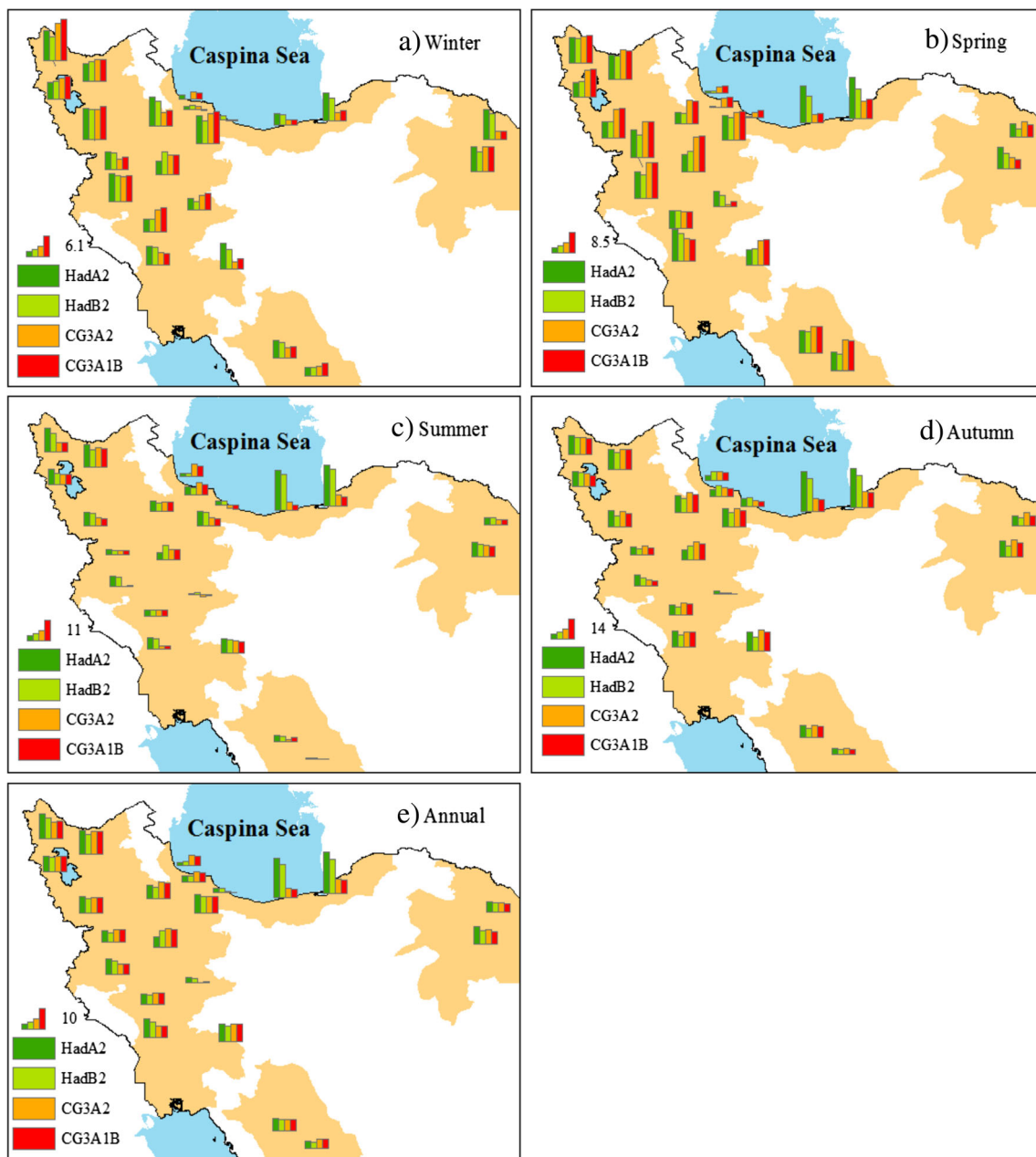


Fig. 6 The ET_0 changes (%) with respect to the baseline period in the study area under HadA2, HadB2, CG3A2, and CG3A1B scenarios in the 2050s

and CG3A1B scenarios, respectively, in the period of the 2020s (the early twenty-first century) (Fig. 5). In the mid-twenty-first century (2041–2070), annual ET_0 was projected to increase by 7.67, 6.75, 9.27, and 8.23%, averaged over all locations, under HadA2, HadB2, CG3A2, and CG3A1B, respectively (Fig. 6). Annual ET_0 will also rise by 13.01, 9.91, 14.80, and 13.08%, averaged across all stations, relative to the baseline period under HadA2, HadB2, CG3A2, and CG3A1B, respectively (Fig. 7), during 2071–2100 (the late twenty-first century). The average annual ET_0 increment was projected to be higher using CGCM3 outputs for most periods and locations. For HadA2 and HadB2 scenarios, Gorgan is anticipated to experience the largest annual ET_0 increase

during the early, mid, and late twenty-first century. Further, the largest increase in annual ET_0 will be occurred in Shahrekord and Tabriz under CG3A2 and CG3A1B scenarios, respectively, for all periods. Under HadA2, the annual ET_0 increase is likely to be the smallest for Ramsar in the 2020s and 2080s and also for Anzali during the 2050s. Moreover, the least annual ET_0 rise was projected for Arak station under HadB2, CG3A2, and CG3A1B scenarios during the twenty-first century. According to the results given in Figs. 5, 6, and 7, the annual ET_0 increment in Arak, west parts of humid region (e.g., Ramsar and Anzali) and southern stations (such as Fassa) would likely be lower as compared to those projected for other stations. Furthermore, a greater increase in annual ET_0 is

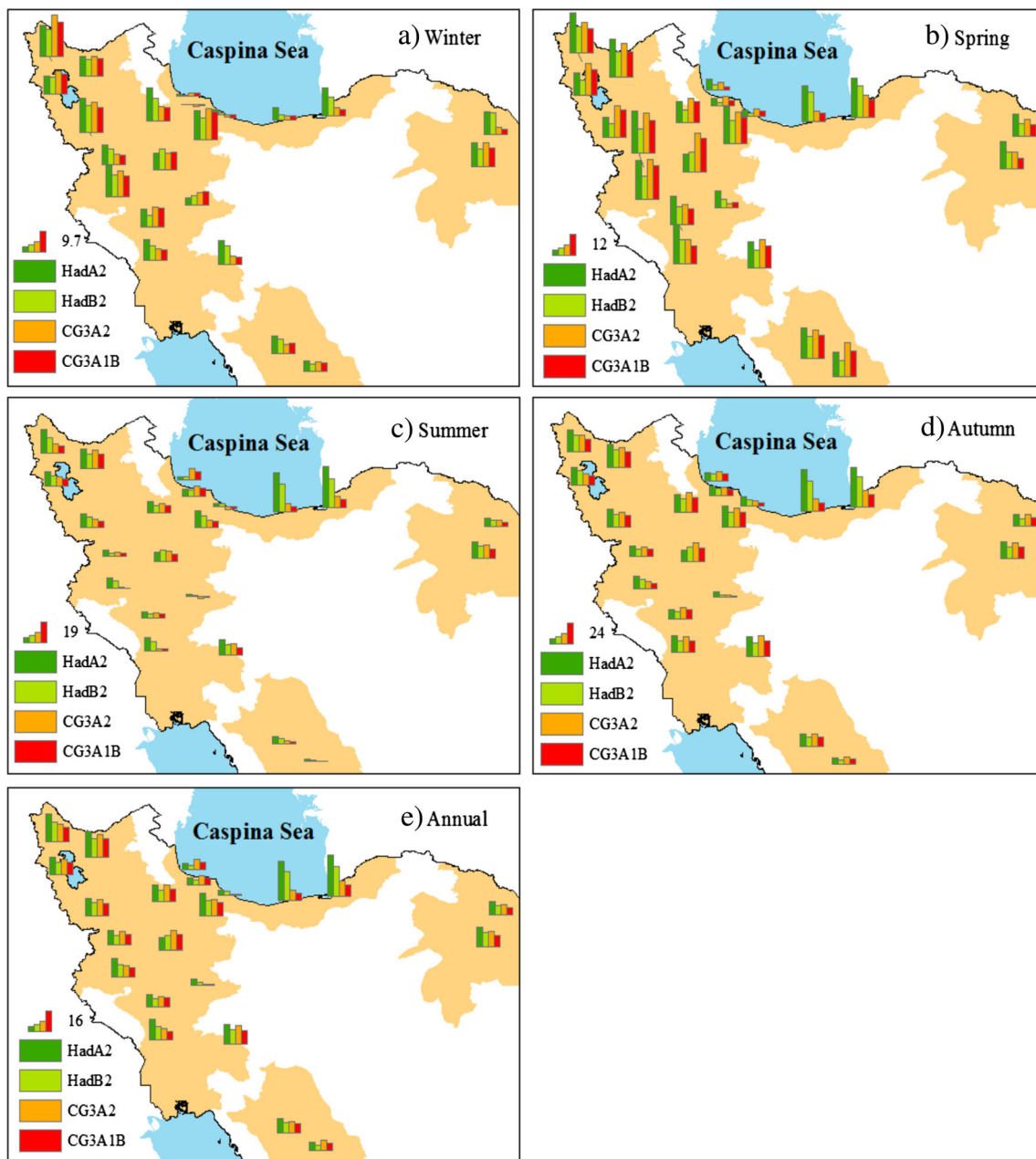


Fig. 7 The ET_0 changes (%) relative to the baseline period in the study area under HadA2, HadB2, CG3A2, and CG3A1B scenarios in the 2080s

anticipated in west and northwest Iran and Babolsar and Gorgan (under HadA2 and HadB2) in the future. Averaged over all stations, the lowest and highest increase was predicted for autumn and summer ET_0 , respectively, under CG3A2 and CG3A1B for all time slices. However, for HadA2 and HadB2 scenarios, the greatest and least seasonal ET_0 increment was modeled during autumn and winter, respectively, over the twenty-first century. The time series of average annual ET_0 for humid and semi-arid from 1966 to 2100 are depicted in Fig. 8. The historical ET_0 series seem to vary more than the projected series. It implies that simulating ET_0 as an exotic variable by statistical downscaling approach mainly provides mean changes of ET_0 rather than its variability in the future.

An increment in T_{mean} and SR and a reduction in RH and U are expected under all scenarios in most time slices (Fig. 9). Averaged across all sites, annual T_{mean} would increase by 10.94, 15.01, and 24.05% under HadA2; 7.54, 12.10, and 17.93% under HadB2; 19.88, 26.65, and 40.33% under CG3A2; and 12.88, 19.98, and 24.99% under CG3A1B during the 2020s, 2050s, and 2080s, respectively, with respect to the baseline period. Hence, T_{mean} is likely to rise continuously through the entire twenty-first century in response to increased GHG emission. In addition, increase of T_{mean} would be larger under CG3A2 and CG3A1B (Fig. 9c, d). Average annual RH will decrease by 5.26, 3.97, and 5.05% for HadA2 scenario; 1.26, 1.77, and 2.88% under HadB2; 7.75, 6.78, and 10.08%

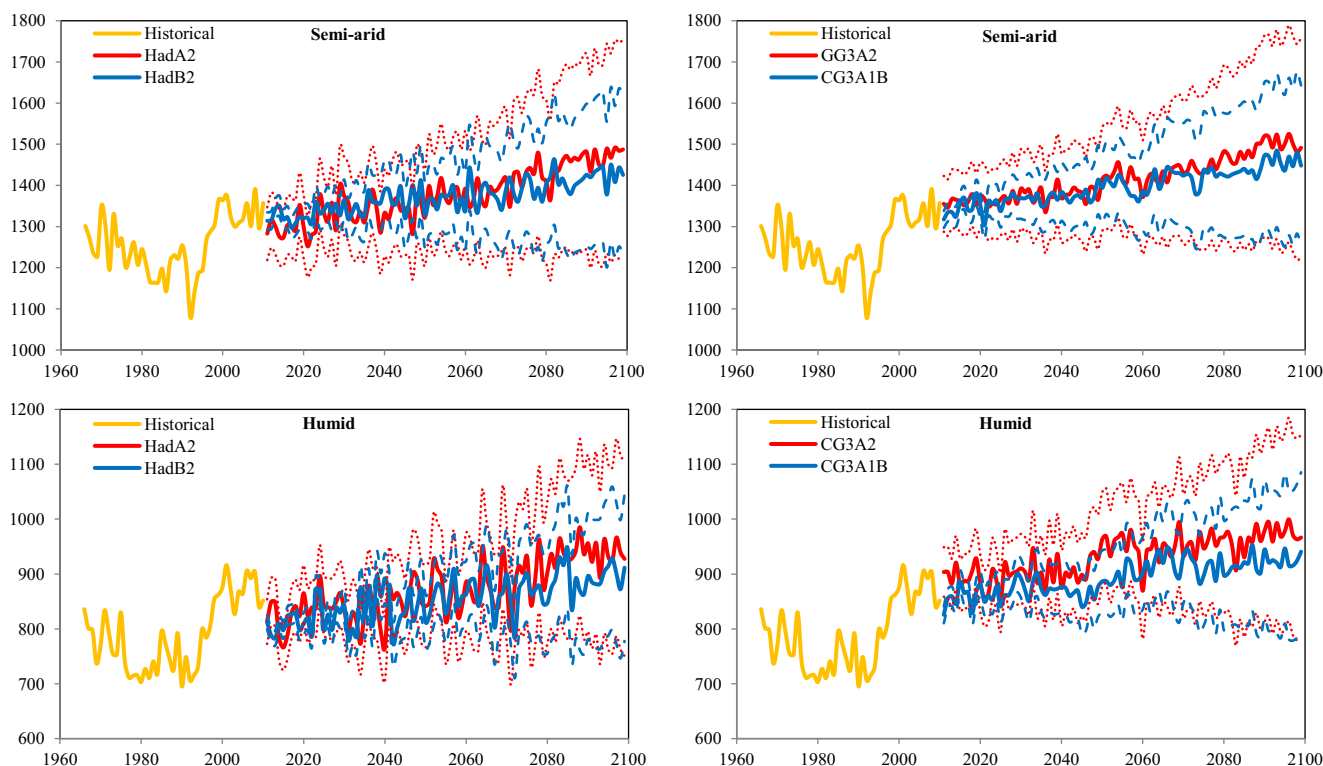


Fig. 8 The average ET_0 series (mm year^{-1}) for semi-arid and humid regions over 1966–2100. The *dotted and dashed series* indicate one standard deviation above and below the mean ET_0

under CG3A2; and 6.56, 5.77, and 8.08% for CG3A1B scenario over the 2020s, 2050s, and 2080s, respectively. The annual RH reduction was projected to be higher under CG3A2 and CG3A1B emission scenarios (Fig. 9c, d). The RH decrease appears to be associated with a likely reduction in precipitation due to CC in the future. As a result, a dried and warmer climate is expected over the studied areas in the twenty-first century. Wind speed (U) would likely decrease by 3.02, 2.92, 6.02, and 4.52% in the 2020s; 2.70, 2.20, 4.20, and 2.20% over the 2050s; and 4.45, 3.67, 6.45, and 3.15% during the 2080s for HadA2, HadB2, CG3A2, and CG3A1B scenarios, respectively, relative to the baseline. The increase of annual SR will not exceed 4%, averaged across all locations, relative to the baseline time period for all scenarios and future time slices (Fig. 9a–d). Although, reduced U may negatively impact ET_0 , ET_0 will rise primarily as a consequence of increased T_{mean} and declined RH through the current century over the studied regions. Wang et al. (2013) also reported T_{mean} and vapor pressure deficit (VPD), a variable associated with RH as the most important variables influencing the future changes of ET_0 on the Tibetan Plateau of China. Considering greater changes of T_{mean} in the future (Fig. 9), enhanced T_{mean} is likely to be the most contributing climatic factor to the ET_0 increase over the twenty-first century. The highest and lowest seasonal T_{mean} rise was, respectively, predicted to occur during autumn and winter under HadA2 and HadB2 (Fig. 9a, b) and during summer and winter

under CG3A2 and CG3A1B scenarios (Fig. 9c, d). The seasons with the largest and smallest projected T_{mean} changes are exactly those with the greatest and least seasonal ET_0 increments. Therefore, seasonal ET_0 changes would be considerably affected by seasonal T_{mean} changes in the future.

Prolonged agricultural droughts mainly caused by enhanced ET_0 and rainfall deficit will adversely influence agricultural outputs and threaten food security in Iran over the coming nine decades (Bannayan and Eyshi Rezaei 2014; Nouri et al. 2016). Since agricultural activities are mostly relied on implementing irrigation in Iran (Alizadeh and Keshavarz 2005), increased future crop water requirements as a result of the ET_0 rise would lead to a severe depletion of water resources in the country. Moreover, the CC-induced increment in ET_0 is likely to create a need for implementing irrigation in dryland agriculture converting rainfed lands to irrigated lands (Cai et al. 2015). Considering increasing trend of environmental and industrial water allocation (Faurès et al. 2007; Molle et al. 2007), recurrent water stress due to surface and groundwater depletion, projected rainfall shortage, and ET_0 increase which will result in more frequent, more intense and longer droughts (Trenberth et al. 2014), large expansion of irrigated lands may not be feasible in the future (Rockström et al. 2010). As a result, adopting appropriate adaptation to manage green water storage (or soil moisture) instead of direct use of blue water (or irrigation) under rainfed condition appears to be of high importance to avoid food insecurity and conserve

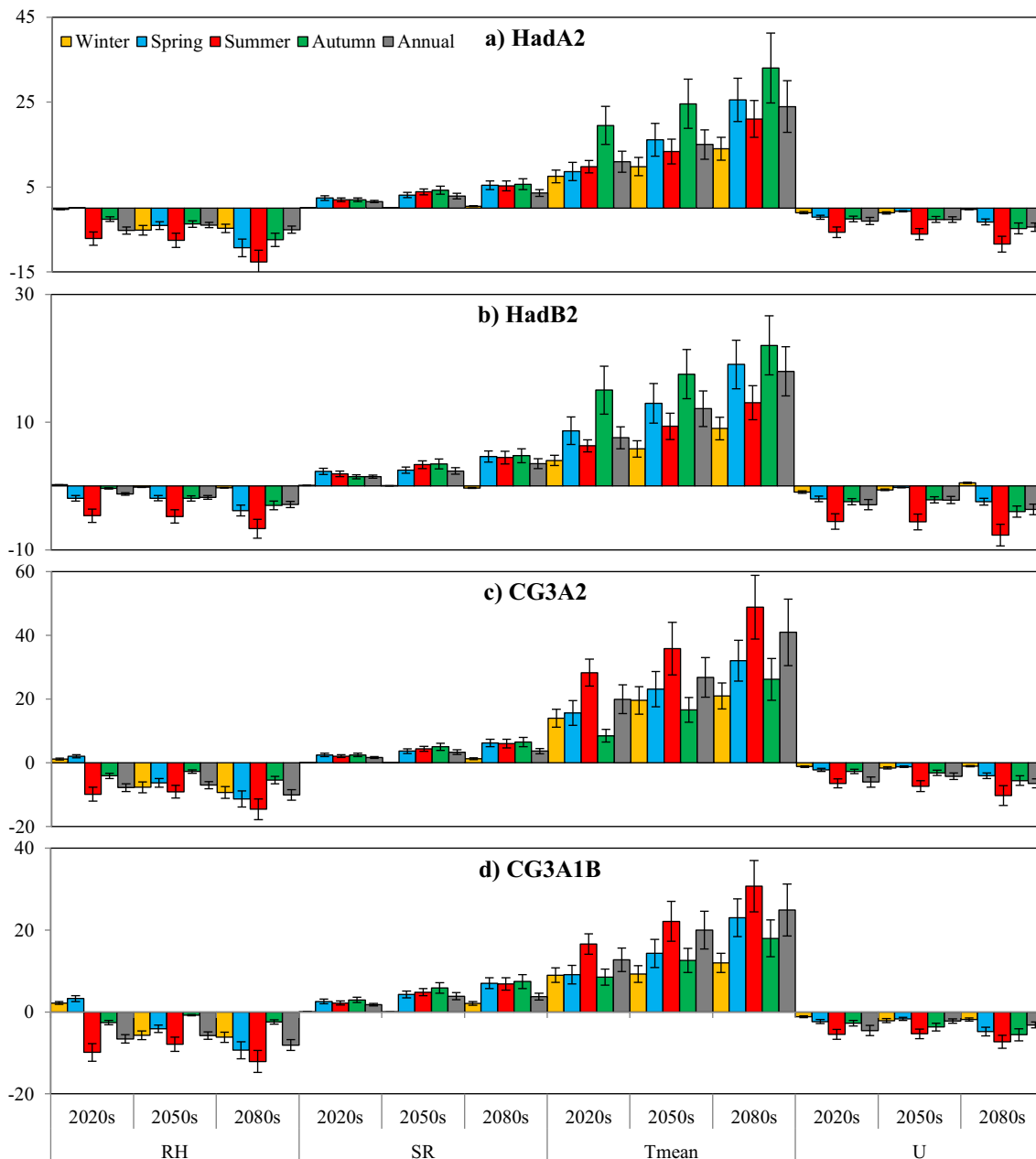


Fig. 9 The changes (%) in U , RH , T_{mean} , and SR during three future time periods relative to the baseline period under the emission scenarios. The error bars show the standard deviation of the mean changes

valuable water resources in Iran under CC (Nouri et al. 2017b). Another implication of the ET_0 increase for water-limited regions is land degradation caused by soil salinization (Homaei and Schmidhalter 2008). The ET_0 increment would cause declined aridity index (P/ET_0) and water surplus ($P-ET_0$) for months in which $P > ET_0$ in the twenty-first century over Iran. Such changes in regional aridity index may change climate particularly for the sites with AI close to 0.2 (boundary value between semi-arid and arid climates based on UNEP (1997)). Zarghami et al. (2011) concluded that climate of Tabriz (a marginal semi-arid region) will likely shift from semi-arid to arid owing to future changes in ET_0 and

precipitation by 2100. Investigating future ET_0 changes seems, therefore, to be a real necessity for identifying proactive adaptation options to reduce the adverse effects of CC on food security and natural resources.

There are inherent uncertainties in projecting CC impacts on hydroclimatic factors mainly generated by emission scenarios, GCMs, hydrological models, and downscaling approaches (Buytaert et al. 2009; Wang et al. 2015; Wilby and Harris 2006). These uncertainties may lead to unreliable final results and consequently jeopardize adaptive strategies and measures. In Fig. 8, ± 1.0 standard deviations of average ET_0 series represent such uncertainties. As discussed earlier, the

ET₀ was downscaled and projected directly by SDSM in this assessment. Thus, the uncertainties in the results can be significantly attributed to nonmeteorological resources which are primarily linked to unrobustness of black box models built by SDSM. Further investigations are also required to provide more details on uncertainties surrounding the ET₀ projection.

4 Conclusions

Our results indicate an increasing trend in annual ET₀ over 1966–2010 in the most studied sites. However, we found a significant trend ($p < 0.05$) only in 36.3% of the studied stations. In addition, insignificant downward trends in ET₀ were identified for southwestern and southern stations mainly due to the decreased wind speed. Wind speed was the most important climatic factor contributing to the ET₀ trend over 1966–2010 in all semi-arid sites. In the studied humid regions, the mean temperature seems to be the key contributor to the ET₀ dynamics. The ET₀ would increase through the twenty-first century in the study area under all emission scenarios. The rise of ET₀ will likely be greater using CGCM3 outputs. The annual ET₀ increment is expected to be lower in western parts of the humid region and southern stations. The average minimum and maximum increase was projected for autumn and summer ET₀, respectively, under CG3A2 and CG3A1B. However, for HadA2 and HadB2 scenarios, the maximum and minimum seasonal ET₀ increment was modeled during autumn and winter, respectively, over the twenty-first century. Temperature would most likely be the main atmospheric variable controlling future ET₀ changes. Decreased aridity index and water surplus, depletion of water resources due to increase of crop water demand, and shifting from rainfed to irrigated cropping systems should be considered as some negative consequences of the ET₀ rise over Iran. Furthermore, serious agricultural drought particularly during autumn and spring caused by increased ET₀ would lead to yield loss and national food insecurity. Overall findings of this study can improve our understanding of negative consequences of climate change and help planners to adopt effective mitigation measures. The uncertainties in the results should be also taken into account by users under decision making processes.

References

- Alizadeh A, Keshavarz A (2005) Status of agricultural water use in Iran. In: Water conservation, reuse, and recycling: Proceedings of an Iranian-American workshop. National Academies Press, Washington DC, pp 94–105
- Allen RG, Pereira LS, Raes D, Smith M (1998) Crop evapotranspiration—guidelines for computing crop water requirements—FAO irrigation and drainage paper 56, vol 300. FAO, Rome, p 6541
- Bannayan M, Eyshi Rezaei E (2014) Future production of rainfed wheat in Iran (Khorasan province): climate change scenario analysis. *Mitigation Adapt Strateg Glob Chang* 19:211–227. doi:10.1007/s11027-012-9435-x
- Bannayan M, Sanjani S, Alizadeh A, Lotfabadi SS, Mohamadian A (2010) Association between climate indices, aridity index, and rainfed crop yield in northeast of Iran. *Field Crops Res* 118:105–114. doi:10.1016/j.fcr.2010.04.011
- Buytaert W, Céleri R, Timbe L (2009) Predicting climate change impacts on water resources in the tropical Andes: effects of GCM uncertainty. *Geophys Res Lett* 36:L07406. doi:10.1029/2008GL037048
- Cai X, Zhang X, Noël PH, Shafiee-Jood M (2015) Impacts of climate change on agricultural water management: a review. *Wiley Interdiscip Rev Water* 2:439–455. doi:10.1002/wat2.1089
- Chu JT, Xia J, Xu C-Y, Singh VP (2010) Statistical downscaling of daily mean temperature, pan evaporation and precipitation for climate change scenarios in Haihe River, China. *Theor Appl Climatol* 99: 149–161. doi:10.1007/s00704-009-0129-6
- Dashtaki SG, Homae M, Khodaverdiloo H (2010) Derivation and validation of pedotransfer functions for estimating soil water retention curve using a variety of soil data. *Soil Use Manag* 26:68–74. doi:10.1111/j.1475-2743.2009.00254.x
- Dettori M, Cesaraccio C, Motroni A, Spano D, Duce P (2011) Using CERES-wheat to simulate durum wheat production and phenology in Southern Sardinia, Italy. *Field Crops Res* 120:179–188. doi:10.1016/j.fcr.2010.09.008
- Dinpashoh Y, Jhajharia D, Fakheri-Fard A, Singh VP, Kahya E (2011) Trends in reference crop evapotranspiration over Iran. *J Hydrol* 399: 422–433. doi:10.1016/j.jhydrol.2011.01.021
- Faurès J-M, Svendsen M, Turrall H, Berkhoff J, Bhattarai M, Caliz A, Darghouth S, Doukkali M, El-Kady M, Facon T (2007) Re-inventing irrigation. In: Molden D (ed) *Water for Food Water for Life: A Comprehensive Assessment of Water Management in Agriculture*. Earthscan and International Water Management Institute, London and Colombo, pp 353–394
- Fowler H, Blenkinsop S, Tebaldi C (2007) Linking climate change modelling to impacts studies: recent advances in downscaling techniques for hydrological modelling. *Int J Climatol* 27:1547–1578. doi:10.1002/joc.1556
- Godfray HCJ, Beddington JR, Crute IR, Haddad L, Lawrence D, Muir JF, Pretty J, Robinson S, Thomas SM, Toulmin C (2010) Food security: the challenge of feeding 9 billion people. *Science* 327:812–818. doi:10.1126/science.1185383
- Golian S, Mazdiyasi O, AghaKouchak A (2015) Trends in meteorological and agricultural droughts in Iran. *Theor Appl Climatol* 119:679–688. doi:10.1007/s00704-014-1139-6
- Held IM, Soden BJ (2006) Robust responses of the hydrological cycle to global warming. *J Clim* 19:5686–5699. doi:10.1175/jcli3990.1
- Homae M, Schmidhalter U (2008) Water integration by plants root under non-uniform soil salinity. *Irrig Sci* 27:83–95. doi:10.1007/s00271-008-0123-2
- Homae M, Dirksen C, Feddes R (2002a) Simulation of root water uptake: I. Non-uniform transient salinity using different macroscopic reduction functions. *Agric Water Manag* 57:89–109. doi:10.1016/S0378-3774(02)00072-0
- Homae M, Feddes R, Dirksen C (2002b) Simulation of root water uptake: III. Non-uniform transient combined salinity and water stress. *Agric Water Manag* 57:127–144. doi:10.1016/S0378-3774(02)00073-2
- Hosseinzadeh Talaei P, Shifteh Some'e B, Sobhan Ardakani S (2014) Time trend and change point of reference evapotranspiration over Iran. *Theor Appl Climatol* 116:639–647. doi:10.1007/s00704-013-0978-x
- Huo Z, Dai X, Feng S, Kang S, Huang G (2013) Effect of climate change on reference evapotranspiration and aridity index in arid region of China. *J Hydrol* 492:24–34. doi:10.1016/j.jhydrol.2013.04.011

- IPCC (2013) Climate change 2013: the physical science basis. Contribution of Working Group I to the Fifth Assessment Report of the Intergovernmental Panel on Climate Change. Cambridge and New York
- Irmak S, Payero JO, Martin DL, Irmak A, Howell TA (2006) Sensitivity analyses and sensitivity coefficients of standardized daily ASCE-Penman-Monteith equation. *J Irrig Drain Eng* 132:564–578. doi:10.1061/(ASCE)0733-9437(2006)132:6(564)#sthash.0bJ7ZZbi.dpuf
- Kistler R, Collins W, Saha S, White G, Woollen J, Kalnay E, Chelliah M, Ebisuzaki W, Kanamitsu M, Kousky V (2001) The NCEP-NCAR 50-year reanalysis: monthly means CD-ROM and documentation. *Bull Am Meteorol Soc* 82:247–267. doi:10.1175/1520-0477(2001)082<0247:TNNYRM>2.3.CO;2
- Kite G, Droogers P (2000) Comparing evapotranspiration estimates from satellites, hydrological models and field data. *J Hydrol* 229:3–18. doi:10.1016/S0022-1694(99)00195-X
- Kousari MR, Ahani H (2012) An investigation on reference crop evapotranspiration trend from 1975 to 2005 in Iran. *Int J Climatol* 32:2387–2402. doi:10.1002/joc.3404
- Li Z, Zheng F-L, Liu W-Z (2012) Spatiotemporal characteristics of reference evapotranspiration during 1961–2009 and its projected changes during 2011–2099 on the Loess Plateau of China. *Agric For Meteorol* 154:147–155. doi:10.1016/j.agrformet.2011.10.019
- Liu Q, Yan C, Ju H, Garré S (2017) Impact of climate change on potential evapotranspiration under a historical and future climate scenario in the Huang-Huai-Hai Plain. *China Theor Appl Climatol*:1–15. doi:10.1007/s00704-017-2060-6
- Molle F, Wester P, Hirsch P, Jensen JR, Murray-Rust H, Paranjpye V, Pollard S, Van der Zaag P (2007) River basin development and management. In: Molden D (ed) *Water for Food Water for Life: A Comprehensive Assessment of Water Management in Agriculture*. Earthscan and International Water Management Institute, London and Colombo, pp 584–624
- Nash JE, Sutcliffe JV (1970) River flow forecasting through conceptual models part I—a discussion of principles. *J Hydrol* 10:282–290. doi:10.1016/0022-1694(70)90255-6
- Nouri M, Homae M, Bannayan M, Hoogenboom G (2016) Towards modeling soil texture-specific sensitivity of wheat yield and water balance to climatic changes. *Agric Water Manag* 177:248–263. doi:10.1016/j.agwat.2016.07.025
- Nouri M, Homae M, Bannayan M (2017a) Quantitative trend, sensitivity and contribution analyses of reference evapotranspiration in some arid environments under climate change. *Water Resour Manag* 31:2207–2224. doi:10.1007/s11269-017-1638-1
- Nouri M, Homae M, Bannayan M, Hoogenboom G (2017b) Towards shifting planting date as an adaptation practice for rainfed wheat response to climate change. *Agric Water Manag* 186:108–119. doi:10.1016/j.agwat.2017.03.004
- Palosuo T, Kersebaum KC, Angulo C, Hlavinka P, Moriondo M, Olesen JE, Patil RH, Ruget F, Rumbaur C, Takáč J (2011) Simulation of winter wheat yield and its variability in different climates of Europe: a comparison of eight crop growth models. *Eur J Agron* 35:103–114. doi:10.1016/j.eja.2011.05.001
- Rahimi J, Ebrahimpour M, Khalili A (2013) Spatial changes of extended De Martonne climatic zones affected by climate change in Iran. *Theor Appl Climatol* 112:409–418. doi:10.1007/s00704-012-0741-8
- Rockström J, Karlberg L, Wani SP, Barron J, Hatibu N, Oweis T, Bruggeman A, Farahani J, Qiang Z (2010) Managing water in rainfed agriculture—the need for a paradigm shift. *Agric Water Manag* 97:543–550. doi:10.1016/j.agwat.2009.09.009
- Sadeghi A, Kamgar-Haghighi A, Sepaskhah A, Khalili D, Zand-Parsa S (2002) Regional classification for dryland agriculture in southern Iran. *J Arid Environ* 50:333–341. doi:10.1006/jare.2001.0822
- Sarmiento JL, Hughes TM, Stouffer RJ, Manabe S (1998) Simulated response of the ocean carbon cycle to anthropogenic climate warming. *Nature* 393:245–249. doi:10.1038/30455
- Sen PK (1968) Estimates of the regression coefficient based on Kendall's tau. *J Am Stat Assoc* 63:1379–1389. doi:10.1080/01621459.1968.10480934
- Seneviratne SI, Corti T, Davin EL, Hirschi M, Jaeger EB, Lehner I, Orlowsky B, Teuling AJ (2010) Investigating soil moisture–climate interactions in a changing climate: a review. *Earth-Sci Rev* 99:125–161. doi:10.1016/j.earscirev.2010.02.004
- von Storch H (1999) Misuses of statistical analysis in climate research. In: von Storch H, Navarra A (eds) *Analysis of Climate Variability: Applications of Statistical Techniques Proceedings of an Autumn School Organized by the Commission of the European Community on Elba from October 30 to November 6, 1993*. Springer Berlin Heidelberg, Berlin, Heidelberg, pp 11–26. doi:10.1007/978-3-662-03744-7_2
- Tabari H, Hosseinzadeh Talaei P (2011) Analysis of trends in temperature data in arid and semi-arid regions of Iran. *Glob Planet Chang* 79:1–10. doi:10.1016/j.gloplacha.2011.07.008
- Trenberth KE, Dai A, van der Schrier G, Jones PD, Barichivich J, Briffa KR, Sheffield J (2014) Global warming and changes in drought. *Nat Clim Chang* 4:17–22. doi:10.1038/nclimate2067
- Türkeş M, Sümer UM (2004) Spatial and temporal patterns of trends and variability in diurnal temperature ranges of Turkey. *Theor Appl Climatol* 77:195–227. doi:10.1007/s00704-003-0024-5
- UNEP (1997) *World atlas of desertification*, Second edn. Arnold, United Nations Environment Programme, London
- Wang W, Xing W, Shao Q, Yu Z, Peng S, Yang T, Yong B, Taylor J, Singh VP (2013) Changes in reference evapotranspiration across the Tibetan Plateau: observations and future projections based on statistical downscaling. *J Geophys Res Atmos* 118:4049–4068. doi:10.1002/jgrd.50393
- Wang W, Xing W, Shao Q (2015) How large are uncertainties in future projection of reference evapotranspiration through different approaches? *J Hydrol* 524:696–700. doi:10.1016/j.jhydrol.2015.03.033
- Wilby RL, Dawson CW (2013) The statistical downScaling model: insights from one decade of application. *Int J Climatol* 33:1707–1719. doi:10.1002/joc.3544
- Wilby RL, Harris I (2006) A framework for assessing uncertainties in climate change impacts: low-flow scenarios for the River Thames, UK. *Water Resour Res* 42:W02419. doi:10.1029/2005WR004065
- Wilby RL, Dawson CW, Barrow EM (2002) SDSM—a decision support tool for the assessment of regional climate change impacts. *Environ Model Softw* 17:145–157. doi:10.1016/S1364-8152(01)00060-3
- Wilby RL, Dawson CW, Murphy C, O'Connor P, Hawkins E (2014) The statistical downScaling model-decision centric (SDSM-DC): conceptual basis and applications. *Clim Res* 61:259–276. doi:10.3354/cr01254
- Xie H, Zhu X (2013) Reference evapotranspiration trends and their sensitivity to climatic change on the Tibetan Plateau (1970–2009). *Hydrol Process* 27:3685–3693. doi:10.1002/hyp.9487
- Xu C-Y, Gong L, Jiang T, Chen D, Singh VP (2006) Analysis of spatial distribution and temporal trend of reference evapotranspiration and

- pan evaporation in Changjiang (Yangtze River) catchment. *J Hydrol* 327:81–93. doi:[10.1016/j.jhydrol.2005.11.029](https://doi.org/10.1016/j.jhydrol.2005.11.029)
- Xu YP, Pan S, Fu G, Tian Y, Zhang X (2014) Future potential evapotranspiration changes and contribution analysis in Zhejiang Province, East China. *J Geophys Res Atmos* 119:2174–2192. doi:[10.1002/2013JD021245](https://doi.org/10.1002/2013JD021245)
- Yang T, Li H, Wang W, Xu CY, Yu Z (2012) Statistical downscaling of extreme daily precipitation, evaporation, and temperature and construction of future scenarios. *Hydrol Process* 26:3510–3523. doi:[10.1002/hyp.8427](https://doi.org/10.1002/hyp.8427)
- Yue S, Pilon P, Phinney B, Cavadias G (2002) The influence of autocorrelation on the ability to detect trend in hydrological series. *Hydrol Process* 16:1807–1829. doi:[10.1002/hyp.1095](https://doi.org/10.1002/hyp.1095)
- Zamani R, Akhond-Ali A-M, Roozbahani A, Fattahi R (2016) Risk assessment of agricultural water requirement based on a multi-model ensemble framework, southwest of Iran. *Theor Appl Climatol* 1–13. doi:[10.1007/s00704-016-1835-5](https://doi.org/10.1007/s00704-016-1835-5)
- Zarghami M, Abdi A, Babaeian I, Hassanzadeh Y, Kanani R (2011) Impacts of climate change on runoffs in East Azerbaijan, Iran. *Glob Planet Chang* 78:137–146. doi:[10.1016/j.gloplacha.2011.06.003](https://doi.org/10.1016/j.gloplacha.2011.06.003)